Magnetic-field-tunable photonic stop band in a three-dimensional array of conducting spheres

M. Golosovsky,* Y. Neve-Oz, and D. Davidov
The Racah Institute of Physics, The Hebrew University of Jerusalem, Jerusalem 91904, Israel
(Received 29 October 2004; published 12 May 2005)

We explore the possibility of tuning photonic crystal properties via order-disorder transition. We fabricated a photonic bandgap material consisting of a three-dimensional array of conducting magnetizable spheres. The spheres self-assemble into ordered state under external magnetic field, in such a way that the crystalline order can be continuously controlled. We study mm-wave transmission through the array as a function of magnetic field, i.e., for different degrees of order. This was done for the regular crystal, as well for the crystal with the planar defect which demonstrates resonance transmission at a certain frequency. We observe that in the ordered, "crystalline" state there is a well-defined stop band, while in the completely disordered, glassy or "amorphous" state, the stop band nearly disappears. We relate the disappearance of the stop band in the disordered state to the fluctuations in the particle area density. We develop a model which predicts how these fluctuations depend on magnetic field and how they affect electrodynamic properties of the whole sample. The model describes our results fairly well.

DOI: 10.1103/PhysRevB.71.195105 PACS number(s): 42.70.Qs, 41.20.Jb, 87.15.Ya

I. INTRODUCTION

Photonic bandgap materials are ordered arrays of scatterers that do not allow electromagnetic wave propagation in some frequency ranges named gaps.[1] The important challenge in the field of photonic crystals is tunability, in other words, the possibility to control the depth, width, and position of these frequency gaps. This can be achieved by various means such as liquid crystal infiltration,[2] temperature,[3] elastic strain,[4] and magnetic field.[5–14] We explore here a very special route to achieve tunable photonic bandgap materials: magnetic-field-induced *order-disorder* transition.

Since the gaps in photonic bandgap materials arise from their periodically ordered structure, we would *a priori* expect that disorder destroys the gaps. However, it is well known that disorder by itself may result in wave localization, i.e., it may create the gap.[15] Hence the effect of disorder on photonic bandgap materials may be multidirectional and it comes to no surprise that it has been studied so intensively recently. Numerous analytical and numerical studies showed that the gaps in photonic crystals are robust,[16–18] i.e., they do not disappear under weak and moderate disorder. More specifically, it was found that under weak disorder the gap edges become smeared,[19–25] the higher-order gaps become more shallow,[26] while the depth of the first stop band remains almost unaffected.[17,18,20–22,24,26] Under moderate disorder the first stop band becomes more shallow.[19,25] Under strong disorder there appear localized states in the gaps, which are characterized by enhanced transmission.[20,21,24] Theoretical predictions indicate that the effect of disorder is most pronounced at the gap edges and is minimal in the passbands, at the frequencies corresponding to the so-called Bragg remnant or antigap.[26–29] Various kinds of disorder (positional disorder, size disorder, fluctuations in refraction index, etc.) produce almost the same qualitative effect. The only exception is sliding disorder (or stacking faults) which can increase the depth of the gap.[22,23]

There are only a few experimental studies of the wave propagation in photonic bandgap materials with disorder. Reference 21 studied microwave propagation through the two-dimensional arrays of rods and found bandgap smearing upon increasing positional disorder, while Ref. 30 studied microwave transmission through random assemblies of spheres and observed wave localization and stop band resulting from disorder. Introduction of small controlled disorder (in fact, "quasicrystalline" order) into two-dimensional photonic bandgap material yields a full photonic stop band in the near infrared.[31,32]

In this work we explore possibility of tuning of photonic bandgap materials by *continuous* variation of the degree of disorder. This is done in the mm-wave range with a model system of metallic magnetizable spheres whose lateral position is controlled by external magnetic field. This resembles the polymer-dispersed liquid crystals where fluctuations in the optical birefringence are controlled by electric field.[33] A similar idea (although based on particle reorientation rather than motion in magnetic field) has been suggested with respect to photonic bandgap materials.[8]

II. EXPERIMENTAL SETUP

A. Photonic crystal with tunable disorder

We build our photonic crystal from the 2 mm diameter steel spheres. In the presence of magnetic field each sphere acquires magnetic moment proportional to the field $M = 3\chi VH/2$, where H is external magnetic field, V is the volume of the sphere, and χ is the magnetic susceptibility. We used SQUID magnetometer to measure particle magnetization in the fields up to 500 Oe and found coercive force of 5 Oe and volume susceptibility $\chi = 0.15$.

We put 397 spheres into a 0.67-mm-thick plexiglas container (Figs. 1 and 2) and mounted several such containers in the stack. The interlayer spacing is 3.5–4.5 mm, while the nearest-neighbor distance in a single layer is 3 mm. The stack is mounted inside the Helmholtz coils. In the presence of external magnetic field the spheres become magnetized in the direction perpendicular to the layers, in such a way that

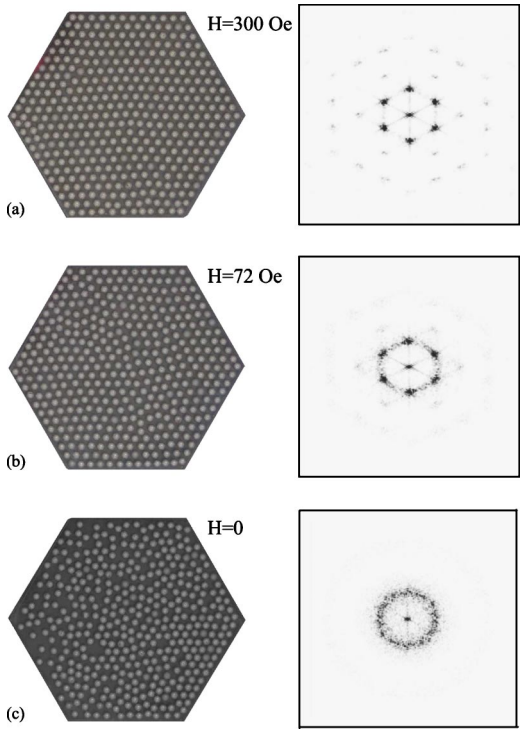

FIG. 1. Particle arrangement in a container at different values of magnetic field. The container is made of a 0.67-mm thin plexiglas plate with the hexagonally shaped walls. The side of a hexagon is 30 mm and there are 397 steel spheres of 2 mm diameter. The left panel shows grey scale images of the particle configuration as obtained by the CCD camera. [The illumination was from above, therefore the actual diameter of the spheres exceeds the diameter of the small white circles in the real space images. In reality, the spheres in (c) touch one another.] Note gradual transition from the ordered to disordered state upon decreasing magnetic field. The right panel shows corresponding Fourier transform image. Note gradual disappearance of sharp peaks and appearance of diffuse rings upon increasing disorder.

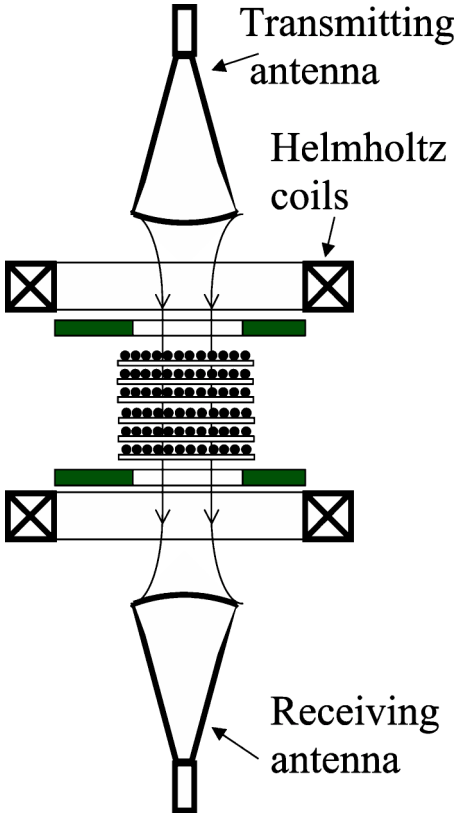

FIG. 2. Measurement setup. A stack of 6–10 layers with steel spheres is mounted inside Helmholtz coils which produce magnetic field perpendicular to the layers. The mm-wave transmission through the stack is measured using standard gain microwave horns connected to HP 8510C Vector Network Analyzer. The antennas are equipped with collimating teflon lenses.

the spheres in each layer repel each other. The out-of-plane attraction between the spheres is small compared to the in-plane repulsion.

The static particle configuration in each layer is determined by the interplay between (i) magnetic forces and (ii) static friction forces between the spheres and the substrate. Under *strong* magnetic field, magnetic forces exceed friction forces and the particles self-assemble into hexagonally ordered crystalline lattice whose orientation is determined by the container shape. Since we use the hexagonally shaped container, and the total number of particles corresponds to the perfect hexagonal packing, the resulting lattice is almost perfect at strong magnetic field [Fig. 1(a)]. At the intermediate magnetic field [Fig. 1(b)], the friction forces deform this crystalline lattice, in such a way that it splits on several crystalline grains separated by grain boundaries. In the weak magnetic field, the friction forces dominate, the particles are in the disordered (amorphous or glassy) state [Fig. 1(c)] and may touch one another.

To characterize disorder we took images of the particle configuration using a CCD camera and then performed digital Fourier-transform of the images. In the strong field we observe sharp Bragg peaks [Fig. 1(a), right panel] indicating on crystalline order; at the intermediate field the intensity of these peaks decreases and the diffuse background appears [Fig. 1(b)]; in the weak magnetic field the Bragg peaks disappear, indicating on the absence of the crystalline order [Fig. 1(c)].

The images of our arrays (Fig. 1) are very similar to the snapshot of the particle configuration in the system of interacting magnetic dipoles at finite temperature.[35] However, instead of temperature, the disordering agent in our case is static friction between the particles and the substrate.

B. mm-wave transmission measurements

We measured mm-wave transmission through our device at normal incidence and in the range of 20–50 GHz. We used a HP850C Vector Network Analyzer as a source and two standard gain horn antennae to which we attached home-made collimating teflon lenses (Fig. 2). The inner curvature of the lens is 15 cm, the outer curvature is 30 cm, the distance between antennas is 28 cm, and the beam diameter is 6 cm. The height of the device is 4–5 cm. To prevent diffraction at the edges of the stack, we put two apertures above and below the stack. The aperture size is slightly smaller than the

container diameter. The receiving antenna accepts radiation in the angle of 25°, hence it measures forward transmission and small angle scattering as well. The noise floor of our setup is −50 dB (measured by replacing a sample with a conducting foil of the same diameter). Calibration was performed without a sample. The size of the particles, the distance between them and the distance between the layers was carefully chosen in such a way as to achieve a wide and deep stop band in the accessible frequency range. This was done by computer simulations using ANSOFT software.

We studied transmission through the stack of 6–10 layers as a function of magnetic field, i.e., at different degrees of in-plane disorder. The measurements were performed as follows. We applied a certain magnetic field to initially disordered array and either gently vibrated it or sent a short current pulse ("magnetic stirring") to achieve equilibration. Then we measured mm-wave transmission through the stack. At the next step we switched off the magnetic field and vibrated the stack once again to recover initial, disordered state. Then we repeated the measurement for another value of magnetic field and so on. While there exist many particular configurations corresponding to a certain value of the external magnetic field, the mm-wave transmission through these metastable configurations differ only in minor details. Therefore, we performed 3–10 vector transmission measurements at the same value of magnetic field and for different particle configurations; and vectorially averaged the results. We also checked experimentally that the transmission through the stack is almost independent of the polarization of the incident wave. A small lateral shift of one of the layers with respect to another (sliding disorder) was also found to be unimportant.

III. EXPERIMENTAL RESULTS

A. Magnetic field dependence of the mm-wave transmission

Figure 3 shows mm-wave transmission through the six-layer stack at two extreme values of magnetic field: one corresponding to completely ordered state, and another corresponding to completely disordered state. In the ordered state there is a well-defined stop band at 24–44 GHz. For the stack with only six layers, the transmission in the stop band is very small, $T=35$ dB. Reflectivity in the stop band is close to unity (not shown here).[34] Transmission in the pass band can be as high as −1–2 dB, indicating on negligible absorption losses. This is not surprising since the losses are determined by the ratio of the skin depth δ in the material of the sphere to its radius r. For the mm-wave frequencies this ratio is so small $\sim 10^{-3}$, that the spheres can be considered ideally conducting, i.e., lossless. The spikes in the stop band in the Fig. 3 do not arise from the noise of the measurement system. They are related to the finite number of layers and to the resonant transmission. The spikes in the magnitude of transmission are accompanied with the similar features in the phase (not shown here).

Upon decreasing magnetic field, the stop band becomes smeared and eventually disappears. Transmission monotonously decreases with decreasing field at all frequencies. The strongest effect of magnetic field is at the stop band edges

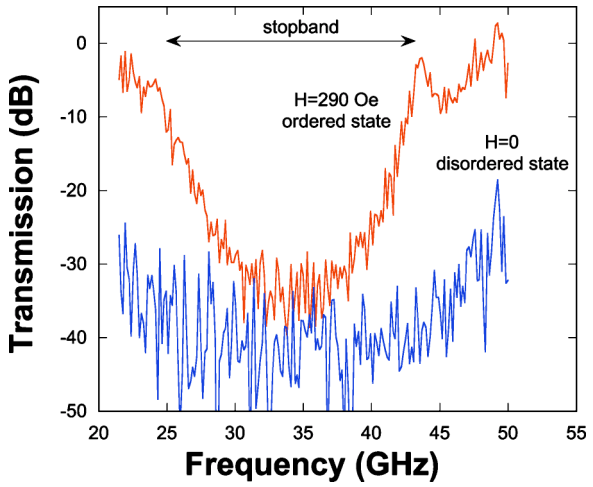

FIG. 3. (Color online) Mm-wave transmission through the six-layer stack for different values of magnetic field. The interlayer separation is $d=3.5$ mm. Note stop band at 25–44 GHz and at $H=290$ Oe (ordered state) and its disappearance in the disordered state ($H=0$).

where it achieves 30 dB; while inside the stop band the magnetic field effect is negligible. Magnetic field effect in the pass band is also quite pronounced. To study it in more detail we prepared a similar stack but with increased interlayer separation. Here, the stop band is shifted to lower frequencies in such a way that the frequency range above the first stop band becomes "visible." Figure 4 shows the effect of magnetic field on the mm-wave transmission in this crystal. The magnetic field effect in the stop band may achieve 15 dB. Note the broad transmission peak between the first and the second stop band in the disordered state, in the frequency range corresponding to the pass band in the ordered state. This peak of enhanced transmission is known as Bragg remnant or antigap.[27–29]

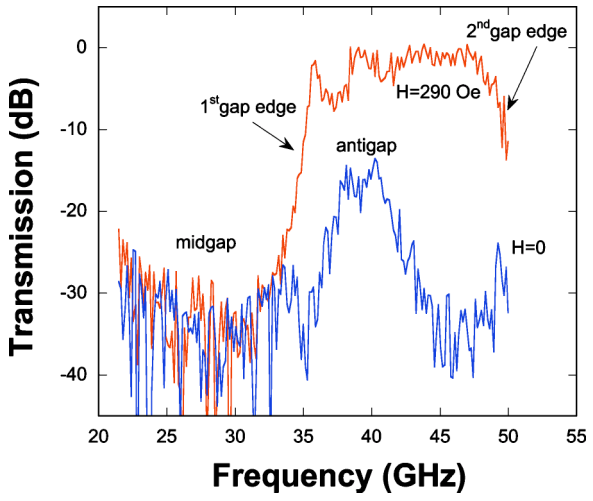

FIG. 4. (Color online) Mm-wave transmission for the similar stack but with increased interlayer distance ($d=4.5$ mm). In the ordered state ($H=290$ Oe) note first stop band at 21–36 GHz and the edge of the second stop band at 46 GHz. Note smearing of the stop band in the disordered state and broad transmission peak at 39 GHz (antigap).

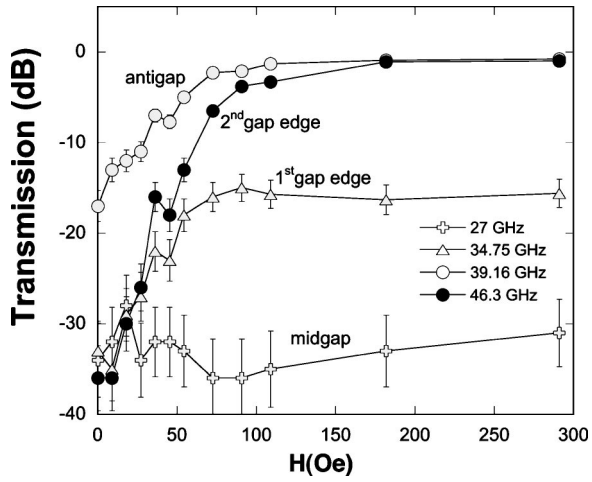

FIG. 5. Magnetic field dependence of the mm-wave transmission through the sample of Fig. 4 and at fixed frequencies. $f=34.7$ GHz corresponds to the high-frequency edge of the first stop band, $f=39.1$ GHz corresponds to the antigap, and $f=46.3$ GHz corresponds to the low-frequency edge of the second stop band.

Figure 5 shows magnetic field dependence of the mm-wave transmission for the sample of Fig. 4 and at few different frequencies, corresponding to the midgap, gap edge, and antigap. Although the overall variation of transmission strongly depends on frequency, the field dependence is much more the same: strong linear increase below 60 Oe followed by saturation at higher field. The only exception is the midgap frequency where the overall change in transmission is so small that its functional dependence cannot be reliably determined.

This can produce a false impression that the mm-wave transmission is totally insensitive to magnetic field for the frequencies corresponding to the midgap. However, this is not exactly so. Figure 6 shows mm-wave transmission through the stack in which we introduced a planar defect, i.e., we displaced two halves of the stack (Fig. 1) in such a way that the distance between two central layers is increased as compared to other interlayer distances. This results in a sharp transmission peak inside the stop band at 34.7 GHz. Upon decreasing magnetic field this peak decreases and completely disappears at $H=0$. The effect of magnetic field on transmission at the resonance frequency amounts to 30 dB. Therefore, magnetic field can strongly affect transmission in the stop band provided this transmission is resonant.

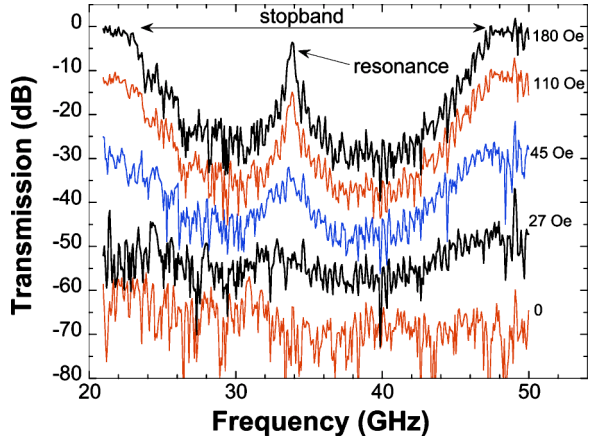

FIG. 6. (Color online) Mm-wave transmission for the same stack as in Fig. 3 but with planar defect (the stack shown in Fig. 1 was split in two parts separated by 6 mm). Note a sharp peak at 34 GHz inside the stop band which corresponds to the resonant transmission. The curves are displaced for clarity.

B. Dispersion relations in the ordered and disordered states

Magnetic field affects not only the magnitude of the transmission (Figs. 3–6) but the phase as well. This means that the phase and group velocity can be magnetically tuned. These velocities are determined from the dispersion relation $k(f)$, where k is the wave vector and f is the frequency. To determine $k(f)$ we performed vector transmission measurements at fixed field and for the stack with varying number of layers N. The real and imaginary parts of the wave vector were found from the experimental data using the following relations:

$$\mathrm{Re}(k)=\frac{1}{d_z}\frac{d\phi}{dN},\ \mathrm{Im}(k)=\frac{1}{2d_z}\frac{d\ln T}{dN}, \tag{1}$$

where T is the power transmission coefficient, ϕ is the phase shift upon transmission, and d_z is the unit cell period in the direction of propagation. Figures 7(a) and 7(b) show our results. In the ordered state, the $\mathrm{Im}(k)$ is very small beyond the stop band, as expected in the lossless material. This is in contrast to the disordered state where the $\mathrm{Im}(k)$ is more or less the same at all frequencies. Note the gap in $\mathrm{Re}(k)$ in the ordered state and the absence of the gap in the disordered state. The group velocity is $v_g=dk/df$. In the disordered state it is fairly frequency independent, while in the ordered state it demonstrates strong frequency dependence, in particular, $v_g\to 0$ at the stop band edges. Therefore, group velocity can be continuously tuned by magnetic field.

IV. MODELING

Although particle configuration in each layer strongly depends on magnetic field, to understand how the changes in configuration affect the mm-wave transmission through the whole sample is not an easy task. Indeed, to explain the appearance of the stop band for the certain direction of propagation in a three-dimensional photonic bandgap material, it is usually enough to represent it as a multilayer with periodicity *only* in the direction of propagation. In this representation the layers are assumed spatially uniform and the details of the particle arrangement in each layer are of little importance. Our idea is that any deviation from the in-plane crystalline order leads to fluctuations in the area density of particles. Therefore, the layer can be no more considered as uniform.

The purpose of our modeling is to find how the in-layer disorder affects the electromagnetic wave propagation perpendicular to the layers. We attribute the effect of lateral disorder to the area density fluctuations. The modeling is performed in three steps. First we estimate fluctuations of the

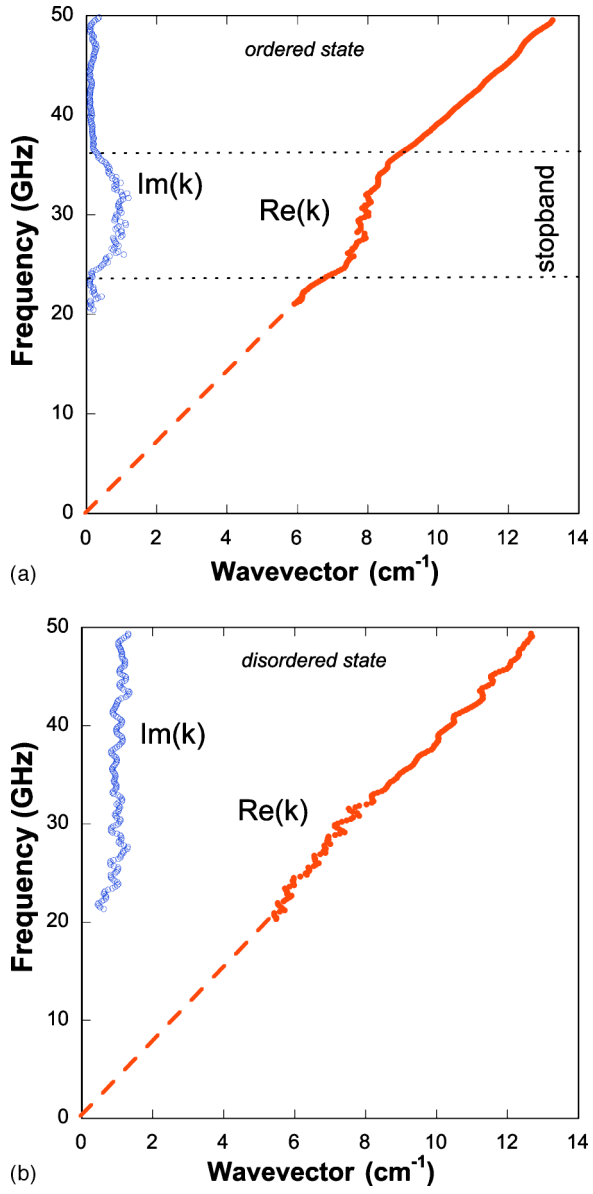

FIG. 7. (Color online) Dispersion relations for the ten-layer stack (331 sphere in each layer, interlayer distance is 4.3 mm). Filled symbols show Re(k) and open symbols show Im(k), where k is the wave vector. The dashed line shows k_0- the wave vector in the uniform medium with the same refraction index as our photonic crystal. (a) The ordered state $H=160$ Oe. (b) The disordered state $H=0$. Note the gap between 24 and 36 GHz in the ordered state and its absence in the disordered state.

particle area density as a function of magnetic field. Secondly, we calculate refraction index and reflectivity of a single layer of spheres with fluctuating area density. Thirdly, we consider wave propagation through the stack of such layers.

A. Magnetic-field-dependent disorder in a layer of magnetizable spheres

Particle configuration in our array is determined by the interplay between magnetic and friction forces. Consider first magnetic forces. The potential energy of induced magnetic dipole-dipole repulsion is

$$U_{ij} = \frac{M_i M_j}{|r_i - r_j|^3}, \tag{2}$$

where r_i is the particle position and M_i is the particle magnetic moment. Magnetic forces $F^i_{\text{magn}} = \Sigma_j (\partial U_{ij}/\partial r_i)$ drive particles into equilibrium hexagonally ordered state where magnetic repulsion energy is minimized and $F^i_{\text{magn}} = 0$. The lattice constant of this array is determined by the number of particles and the size and shape of container.[12] Since magnetic susceptibility of our spheres is not high, we assume $M \propto H$ where H is *external* field (rather than the sum of the external field and the induced field of other particles).

To achieve equilibrium, the particles should move laterally. Here, static friction forces become important. Indeed, to push a hard sphere on flat substrate out of equilibrium requires application of some mimimal force, exceeding static friction force $F_{\text{fr}} = \mu_{\text{fr}} P$, where P is normal force on a particle and μ_{fr} is the rolling friction coefficient which depends on the radius of the sphere and on the nature of contacting surfaces. In the presence of static friction the particles start to move only when $F_{\text{magn}} > F_{\text{fr}}$ and come to rest when $F_{\text{magn}} \leqslant F_{\text{fr}}$. To characterize the interplay between magnetic and friction forces we introduce "magnetic length" $2l_H$ that represents a minimal distance between two isolated magnetized spheres on substrate with friction. We find it from the relation $F_{\text{magn}}(2l_H) = F_{fr}$. Equation (2) yields

$$l_H = \left(\frac{3M^2}{16 F_{\text{fr}}} \right)^{1/4}. \tag{3}$$

In this work we are interested in the magnetizable particles ($M \propto H$), hence $l_H \propto H^{1/2}$. The magnetic length should be compared to the average distance between the particles. The latter is conveniently characterized by the Wigner-Seitz radius $a = (\pi\rho)^{-1/2}$, where ρ is the area density of the particles. Note that l_H is controlled by magnetic field [Eq. (3)] while a is field independent. In what follows we consider different regimes, defined by the relation between l_H and a.

1. Strong magnetic field (crystalline state)

Here $l_H \gg a$. Magnetic repulsion tends to keep the particles at equal distances. For confined array and at high enough field this results in the hexagonally ordered "crystalline" state. The whole array is a single crystallite (with probably few point defects) which is deformed by friction forces. In the absence of point defects such as dislocations and disclinations,[36,37] we estimate the area density fluctuations arising from elastic deformations as follows. The condition of static equilibrium of the elastically deformed planar crystalline lattice is

$$\frac{\partial \sigma_{ik}}{\partial x_k} + \rho f_i = 0. \tag{4}$$

Here σ_{ik} is the stress tensor and f_i is the density of bulk external forces which in our case are friction forces. The magnitude of these forces is F_{fr}. We assume that their corre-

lation radius is the Wigner-Seitz radius a. By integrating Eq. (4) over unit cell, we find $|\sigma_{ik}| \approx \rho F_{\mathrm{fr}}\, a$. The compressional deformations are $|u_{ll}| \sim \rho F_{\mathrm{fr}}\, a/K$, while the shear deformations are $|u_{ik}| \sim \rho F_{\mathrm{fr}}\, a/\mu$, $(i \neq k)$. Here, K is the bulk compression modulus and μ is the shear modulus. For the planar hexagonal lattice of parallel magnetic dipoles[36]

$$\mu = \frac{2.147M^2}{a^5}, \quad K = 10\mu. \tag{5}$$

Equations (3) and (5) yield fluctuations of the deformations $|u_{ll}| \approx 2.75 \times 10^{-3}(a/l_H)^4$, $|u_{ik}| \approx 10|u_{ll}|$. The corresponding density fluctuations are very small:

$$\frac{\overline{\delta\rho^2}}{\rho^2} \sim \overline{u_{ll}^2} \propto \left(\frac{a}{l_H}\right)^8 \propto H^{-4}. \tag{6}$$

2. Intermediate field (polycrystalline state)

Here $l_H > a$. In this regime, the friction forces between the particles and the substrate are strong enough to split the crystalline lattice onto separate grains with well-defined grain boundaries. To estimate the grain size R, we follow Larkin-Ovchinnikov treatment of the pinned vortex lattice in superconducting films.[38] The maximum energy, associated with one particle in the lattice pinned by friction force, is $\sim F_{\mathrm{fr}}\, a$. Since the friction forces are randomly oriented, the average pinning energy for the grain of area πR^2, containing $Z_g = (R/a)^2$ particles, is $\sim F_{\mathrm{fr}}\, a Z_g^{1/2} = F_{\mathrm{fr}} R$. These pinning forces lead to displacement of the grain boundary by $\sim a$. The elastic energy associated with this displacement is $\sim \mu a^2$. The excess energy per unit area of such lattice is

$$\frac{\delta E}{S} \sim \frac{\mu a^2 - F_{\mathrm{fr}} R}{\pi R^2}. \tag{7}$$

Since $K \gg \mu$ we neglect here the elastic energy due to compressional deformations. Minimization of Eq. (7) yields the equilibrium grain size $R = 2\mu a^2/F_{\mathrm{fr}}$. Using Eqs. (3) and (5) we find the grain size

$$R \approx 22.4 \frac{l_H^4}{a^3} \propto H^2. \tag{8}$$

To estimate density fluctuations we note that the lattice in the grains is almost perfect, while the particle configuration at grain boundaries is distorted and strong deformations u_{ik} occur there [Fig. 1(b)]. In other words, $u_{ik} \ll 1$ in the grains and $u_{ik} \sim 1$ at grain boundaries. The relative concentration of grain boundary particles is $Z_B \approx 2a/R$. The average fluctuation of the deformations in the area S, containing $Z_S = \rho S$ particles, is

$$\overline{u_{ik}^2} \sim \frac{Z_B}{Z_S} \sim \frac{0.09}{Z_S}\left(\frac{a}{l_H}\right)^4 \propto H^{-2}. \tag{9}$$

3. Weak magnetic field (amorphous state)

Here $l_H \ll a$. The particle arrangement reminds a glass or amorphous solid consisting of impenetrable spheres with the radius l_H. The area density fluctuation in the area S containing Z_S particles is[39]

$$\frac{\overline{\delta\rho^2}}{\rho^2} = \frac{\overline{\Delta Z_S^2}}{Z_S^2} = \frac{1 + \int \nu\, \partial S}{Z_S}, \tag{10}$$

where ν is the pair correlation function. Following Ref. 40, we assume that the correlation function for the dense disordered planar array of impenetrable spheres of radius r is such that $\int \nu \partial S \approx -\pi\rho r^2$. We substitute r by l_H, ρ by $1/\pi a^2$, introduce these values into Eq. (10) and find

$$\frac{\overline{\delta\rho^2}}{\rho^2} = \frac{1 - \dfrac{l_H^2}{a^2}}{Z_S}. \tag{11}$$

Since $l_H \propto H^{1/2}$, the Eq. (11) yields density fluctuations linearly decreasing with H. Note, that if $l_H < r$, where r is the radius of the sphere, the magnetic forces are too small as compared to friction forces, and magnetic field is inoperative.

B. Electrodynamic parameters of a planar array of conducting spheres

We consider first an ordered planar array of ideally conducting spheres of radius r, such that $r < \lambda/2\pi$, where λ is the wavelength of the incident wave (such spheres can be considered as Rayleigh scatterers). The average nearest-neighbor distance is smaller than $\lambda/2$. When the planar electromagnetic wave is incident on such a layer, it is not absorbed but scattered. The scattering occurs mostly in the backward and forward directions, while the scattering in oblique directions is strongly suppressed. Therefore, for the normally incident plane wave this layer can be considered as a uniform nonabsorbing medium with thickness $d = 2r$, effective refraction index n and admittance Y.[41] For dilute arrays of scatterers the Refs. 42 and 43 yield

$$n \simeq 1 - i2\pi \frac{\rho S(0)}{k^3 d}, \tag{12}$$

$$Y \simeq 1 - i2\pi \frac{\rho S(180)}{k^3 d}. \tag{13}$$

Here, ρ is the area density of particles; and admittance Y is normalized to the admittance of free space. The $S(0)$ and $S(180)$ are the forward and backward scattering amplitude of a single particle, correspondingly, which are related to their electric α_E and magnetic α_H susceptibilities as follows:[42,43]

$$S(0) = ik^3(\alpha_E + \alpha_H), \quad S(180) = ik^3(\alpha_E - \alpha_H). \tag{14}$$

The susceptibilities depend on particle concentration due to Lorentz field. Indeed, the susceptibility of a polarizable dipole in the array of identical dipoles is

$$\alpha = \frac{\alpha_0}{1 - A\dfrac{\alpha_0}{a^3}}. \tag{15}$$

Here α_0 is the susceptibility of an isolated particle (for a small isolated ideally conducting sphere, $\alpha_E = r^3$, $\alpha_H = -r^3/2$);

$a=(\pi\rho)^{-1/2}$ is the Wigner-Seitz radius, and A is a local field factor.[44] To find refraction index and admittance of a planar *ordered* array of ideally conducting spheres, we substitute Eq. (15) into Eqs. (12)–(14) and find

$$n \simeq 1 + \frac{x^2(1+2Ax^3)}{(1-Ax^3)(2+Ax^3)}, \tag{16}$$

$$Y \simeq 1 + \frac{3x^2}{(1-Ax^3)(2+Ax^3)}, \tag{17}$$

where $x=r/a$. Note that n, Y depend on density (through x and a).

To find refraction index and admittance of the planar disordered array of ideally conducting spheres we represent it by the ordered array with the spatially varying density $\rho=\rho_0+\delta\rho$. The Taylor expansion of Eqs. (16) and (17) with respect to ρ yields

$$n(\rho) \simeq n(\rho_0) + \frac{dn}{d\rho}\delta\rho + \frac{d^2n}{d\rho^2}\frac{\delta\rho^2}{2}\cdots, \tag{18}$$

$$Y(\rho) \simeq Y(\rho_0) + \frac{dY}{d\rho}\delta\rho + \frac{d^2Y}{d\rho^2}\frac{\delta\rho^2}{2}\cdots. \tag{19}$$

To find n, Y in the disordered state we use the same Eqs. (18) and (19) and substitute $\delta\rho^2$ by area density fluctuations. Then we average over the area S which scatters coherently. Its size is $S=z\lambda$ where z is the distance to the observation point and λ is the wavelength. (When the averaging is performed over whole array, $\langle\delta\rho\rangle=0$, but $\langle\delta\rho^2\rangle\neq 0$.)

The above approach reduces the effect of disorder on n, Y to the area density fluctuations. When the array of particles is ordered, this corresponds to compressional deformations. However, disorder introduces shear deformations as well. These deformations change local crystalline symmetry and this affects refraction index and admittance through the local field factor A.[40,44] In principle, the effect of shear deformations may be treated along the same lines by considering Taylor expansion of Eqs. (16) and (17) with respect to A.

C. Electrodynamic parameters of the multilayer with in-plane disorder

We represent our sample as a multilayer consisting of alternating layers of conducting spheres and air spacings between them. Wave transmission through multilayers is most easily accounted for by the matrix method.[45,46] Here, each layer is characterized by two matrices: (i) the phase matrix representing the phase shift upon transmission through this layer and (ii) the reflectivity matrix which is determined by the ratio of admittances at the reflecting interface and is independent of the layer thickness. Transmission through the multilayer is the product of all these matrices. We relate the effect of disorder on transmission through our multilayer to the area density fluctuations in the layers of conducting spheres. We assume that the lateral size of important fluctuations corresponds to the area that radiates coherently, as seen from the next interface, i.e., $S\sim\lambda d_z$ where d_z is the unit cell period in the direction of propagation and λ is the wavelength. In what follows we consider the effect of area density fluctuations in different frequency ranges.

1. Antigap

The antigap is the narrow frequency range in the passband where the layer of spheres may be represented as a half-wavelength plate, i.e., the phase shift on propagation through this layer is a muliple of π. Transmission through such layer is close to unity due to destructive interference of the waves reflected from both interfaces and is almost independent on the layer admittance. Transmission at the antigap frequency is, therefore, determined mostly by refraction index fluctuations across the layers [Eq. (18)]. The latter result in the phase shift fluctuations $\psi=\psi_0+\delta\psi$. The power transmission through the multilayer decreases by the Debye-Waller factor $T_{\text{disorder}}/T_{\text{order}}=e^{-\overline{\delta\psi^2}}$.[47] What is important here is the relative deviation of the phase shift when going from one layer to another. Hence, the averaging in the exponent is for different layers, i.e. for different realizations of the disordered state. Since $\psi=k_0nd$, where k_0 is the free space wave vector, then $\delta\psi=k_0d\delta n=k_0d(dn/d\rho)\delta\rho$. Hence, the ratio of transmittances for the N-layer stack is

$$\left(\ln\frac{T_{\text{disorder}}}{T_{\text{order}}}\right)_{\text{antigap}} = -N\left(k_0d\frac{dn}{d\rho}\right)^2\overline{\delta\rho^2}. \tag{20}$$

Note that the ratio of transmittances is $\propto k_0^2$, i.e., increases with frequency. Therefore the effect of disorder is more pronounced in the higher-order passbands.

2. Midgap

In the midgap the reflected waves from all interfaces sum up in phase, hence the reflectivity is maximal and transmission is minimal. For simplicity, we restrict ourselves to the first stop band and to the quarter-wavelength stack. Transmission through such stack is $T\approx 1/Y^{2N}$,[46] where N is the number of layers. The average admittance of each layer in the disordered state is $Y_{\text{disorder}}=Y_{\text{order}}+(d^2Y/d\rho^2)\overline{\delta\rho^2}$ where the averaging is performed over the whole layer. This results in

$$\left(\ln\frac{T_{\text{disorder}}}{T_{\text{order}}}\right)_{\text{midgap}} = -\frac{N}{Y}\frac{d^2Y}{d\rho^2}\overline{\delta\rho^2}. \tag{21}$$

3. Stop band edges

To account for the effect of disorder on the transmission at gap edges we draw analogy to the optical properties of disordered semiconductors. Upon increasing disorder, the gap in semiconductors becomes smeared and there appear exponential transmission tails at gap edges (Urbach tails). The frequency dependence of optical transmission through semiconductors and at the gap edge is[48]

$$\frac{\partial\ln T}{\partial f} \propto \overline{\delta a_L^2}, \tag{22}$$

where $\overline{\delta a_L^2}$ is the lattice constant variation which can arise from structural or temperature fluctuations. We rewrite Eq.

(22) for a single frequency, and note that $\delta a_L/a_L=\delta\rho/2\rho$. Then Eq. (22) yields the ratio of the transmissions in the ordered and disordered states at any frequency corresponding to the gap edge as

$$\left(\ln\frac{T_{\text{disorder}}}{T_{\text{order}}}\right)_{\text{edge}} \propto \overline{\delta\rho^2}. \tag{23}$$

4. Scattering

In addition to the frequency-selective effects considered in previous subsections, there is also scattering that decreases transmission at all frequencies.[24,49] These extinction losses are also proportional to density fluctuations[42]

$$\left(\ln\frac{T_{\text{disorder}}}{T_{\text{order}}}\right)_{\text{scattering}} \propto \overline{\delta\rho^2}. \tag{24}$$

We observe that Eqs. (20), (21), (23), and (24)—all yield exponential dependence of the transmission on density fluctuations

$$\ln\frac{T(f,H)}{T_{\text{ord}}} = -B(f)\frac{\overline{\delta\rho^2(f,H)}}{\rho^2}, \tag{25}$$

where T_{ord} is the transmission in the completely ordered state and $B(f)$ is the frequency-dependent prefactor. Equation (25) assumes monotonous dependence of transmission on disorder. This is valid only for the relatively weak disorder, while for the strong disorder this dependence can be nonmonotonous in certain frequency ranges.[19]

V. COMPARISON TO EXPERIMENT

A. Magnetic-field dependent order-disorder transition

We explore magnetic field dependence of the in-plane disorder. We quantify disorder through the intensity of diffuse rings in the Fourier transform images (Fig. 1). As it is well-known from the x-ray structure analysis, I_{diff} is directly related to the lattice constant fluctuations, which are closely related to the density fluctuations, i.e., $I_{\text{diff}}\propto\overline{\delta\rho^2}/\rho^2$. At Figs. 8 and 9 we plot I_{diff} in dependence of magnetic field. Here, we set $I_{\text{diff}}=1$ in the completely disordered state, i.e., at $H=0$. In the weak field the data can be well approximated by the linear dependence $I_{\text{diff}}=1-\beta H$ as predicted by Eq. (11) for the amorphous state. At higher field, the data are fairly well approximated by the $1/H^2$ dependence (see also Fig. 9), as predicted by Eq. (9) for the polycrystalline state.[60] The crossover between these two regimes occurs at $H=50$–60 Oe. This corresponds to the field when the Bragg peaks in the Fourier transform image are replaced by diffuse rings (Fig. 1) and is suggestive of some kind of melting or glass transition.[50–54]

B. mm-wave transmission through the regular crystal

To verify relation between transmission and area density fluctuations, as predicted by Eq. (25), we plot them together versus magnetic field (Figs. 8 and 9). Both $I_{\text{diff}}(H)$ and $T(H)$ dependences collapse on one curve. This means that $T(H)$ is indeed proportional to I_{diff} and to the density fluctuations, as predicted by Eq. (25). This is the central result of our paper.

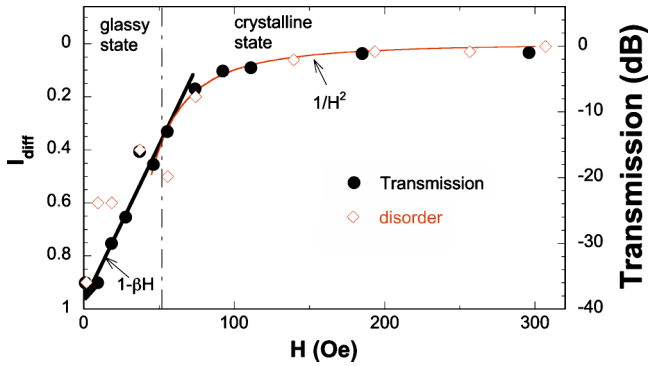

FIG. 8. (Color online) Mm-wave transmission at 46.3 GHz for the sample of Fig. 5 (filled circles) and the intensity of diffuse background (open rhombs) I_{diff} estimated from the Fourier-transform images of Fig. 1. Straight solid line shows linear dependence as predicted by Eq. (11) for the glassy state; the thin curved line shows $1/H^2$ dependence as predicted by Eq. (9) for the polycrystalline state. The vertical line delineates the strong field region (where Fourier transform imaqe of Fig. 1 shows sharp Bragg peaks, indicating on crystalline state), from the weak field region (here Fourier transform imaqe of Fig. 1 shows sharp diffuse rings indicating on amorphous or glassy state).

The absolute value of the fluctuations in the completely disordered state may be estimated as follows. Equation (11) predicts that at $H=0$, $\overline{\delta\rho^2}/\rho^2\approx 1/Z_S$. Since $Z_S=\rho d_z\lambda$, we substitute $\rho=0.17$ mm^{-2}, $d_z=4.5$ mm, $\lambda=6$–15 mm, and find $Z_S\approx 5$–11 depending on frequency. This corresponds to $\overline{\delta\rho^2}/\rho^2=0.1$–$0.2$.

Since our model accounts fairly well for the magnetic field dependence of the mm-wave transmission, in what follows we only estimate the prefactor $B(f)$ in Eq. (25). To this end we compare the ratio of transmittances in the completely ordered and in the completely disordered states and for cer-

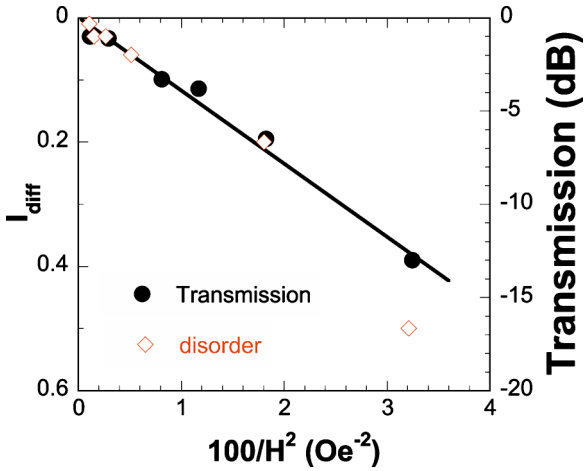

FIG. 9. (Color online) A different representation of the high-field data of Fig. 8. Filled circles show mm-wave transmission at 46.3 GHz for the sample of Fig. 5, open rhombs show the magnitude of area density fluctuations I_{diff}. Straight solid line shows linear dependence on $1/H^2$ as predicted by Eq. (9).

tain frequencies. In particular, for the antigap, we substitute into Eq. (20) $N=6$, $f=46$ GHz, $\overline{\delta\rho^2}/\rho^2=0.2$, $a=1.37$ mm, $x=0.73$, $A=0.5$, $n=1.4$, $\rho dn/d\rho=0.7$ and find $\ln T_{\text{disorder}}/T_{\text{order}}=-24$ dB. This should be compared to the experimentally observed value of -10–15 dB (Fig. 4). For the *midgap*, we substitute into Eq. (21), $N=6$, $f=27$ GHz, $\overline{\delta\rho^2}/\rho^2=0.12$, $x=0.73$, $A=0.5$, $Y=1.9$, $\rho^2 d^2Y/d\rho^2=0.4$ and find $\ln T_{\text{disorder}}/T_{\text{order}}=-2.5$ dB. This should be compared to the observed value of ~ -5 dB (Figs. 3 and 4).

We conclude that our model qualitatively predicts field dependence of the transmission through disordered photonic crystal. To achieve better quantitative agreement, there is need in a more advanced model of the kind suggested by Ref. 55. This model should go further than Eqs. (12), (13), (16), and (17) which assume low concentration of scatterers and Rayleigh scattering regime. The model should also account for the quadrupole interactions between magnetized particles.

C. mm-wave transmission through the crystal with a planar defect

The microwave transmission through the crystal with a planar defect can be treated following the same lines. We consider the photonic crystal split on two halves, as two photonic crystals coupled through the Fabry-Perot resonator. Transmission through this device is[34]

$$T_{\text{FP}}=\frac{e^{i(2\pi f\Delta/c)}S_{12}^2}{e^{i(4\pi f\Delta/c)}-S_{11}^2}, \tag{26}$$

where Δ is the spacing between the mirrors and S_{12} and S_{11} are complex transmission and the reflection coefficients for each of the halves (note that S_{11} and S_{12} are interrelated and both are affected by disorder). The resonant transmission through such a crystal is possible provided the denominator of Eq. (26) is small, i.e., $1-|S_{11}|^2 \ll 1$. Even small disorder strongly affects this condition, hence the transmission through the defect drops dramatically in the disordered state (Fig. 6).

VI. DISCUSSION AND CONCLUSIONS

Continuous variation of electromagnetic properties of our samples when external magnetic field goes to zero closely resembles the change of optical properties of liquids upon approaching the critical point. Indeed, the optical transmission at the critical point is very small due to enhanced density fluctuations. According to Einstein's theory, the density fluctuations inversely depend on compressibility which goes to zero at the critical point.[47] The compressibility of our array of magnetizable spheres, $K^{-1}\sim 1/H^2$ [Eq. (5)], also diverges when $H\to 0$. The density fluctuations, as it is shown by Eq. (9), increase accordingly.

Our experiments bear some resemblance to the studies of electromagnetic wave propagation through ferrofluids.[56,57] Indeed, in the absence of magnetic field the particles in ferrofluid are in the disordered state, while in the presence of magnetic field they self-assemble into chains. This results in field-induced anisotropy which strongly affects the polarization of the electromagnetic wave propagating through such a media. However, in 3D, magnetic field does not induce the long-range order in ferrofluids, hence the field-induced anisotropy is frequency independent. This is very different from our present experiment where magnetic field drives the particle array into crystalline state with a long-range order, and this has a strong frequency-selective effect on the microwave transmission. However, two-dimensional ferrofluid layers[58,59] bear strong resemblance to our system.

In summary, we demonstrate a metallodielectric photonic crystal exhibiting stop band in the mm-wave range. Mm-wave transmission through this crystal can be controlled by external magnetic field through magnetic field-induced order-disorder transition. We develop a physical model which describes our experimental data fairly well. Our concepts may be useful in interpretation of the effect of disorder in photonic bandgap materials. Our results can be useful for the fabrication of tunable planar photonic crystals, based on surface waves, in particular surface plasmons. If the surface is covered with the liquid layer containing movable magnetic particles, (especially when this layer represents a photonic crystal with a tunable lattice constant) the propagation of the surface waves can be effectively monitored.

ACKNOWLEDGMENTS

This work was supported by the VW Foundation, Israeli Science Foundation, and Israeli Ministry of Science and Technology. We are grateful to I. Felner for magnetization measurements; to A. Frenkel for the help with computer simulations; and to B. Laikhtman, L. Schvartsman, A. Sarychev, and V. Freilikher for fruitful discussions.

*Email address: golos@vms.huji.ac.il

[1] J. D. Joannopoulos, R. D. Meade, and J. N. Winn, *Photonic Crystals Molding the Flow of Light* (Princeton University Press, Princeton, 1995).
[2] K. Busch and S. John, Phys. Rev. E **58**, 3896 (1998).
[3] P. Halevi and F. Ramos-Mendieta, Phys. Rev. Lett. **85**, 1875 (2000).
[4] S. Kim and V. Gopalan, Appl. Phys. Lett. **78**, 3015 (2001).
[5] I. L. Lyubchanskii, N. N. Dadoenkova, M. I. Lyubchanskii, E. A. Shapovalov, and Th. Rasing, J. Phys. D **36**, R277 (2003).
[6] V. I. Belotelov and A. K. Zvezdin, J. Opt. Soc. Am. B **22**, 286 (2002).
[7] B. Gates and Y. N. Xia, Adv. Mater. (Weinheim, Ger.) **13**, 1605 (2001).
[8] A. Figotin, Y. A. Godin, and I. Vitebsky, Phys. Rev. B **57**, 2841 (1998).
[9] X. L. Xu, G. Friedman, K. D. Humfeld, S. A. Majetich, and S. A. Asher, Adv. Mater. (Weinheim, Ger.) **13**, 1681 (2001).

[10] C. Xu, X. Hu, Y. Li, X. Liu, R. Fu, and J. Zi, Phys. Rev. B **68**, 193201 (2003).
[11] E. L. Bizdoaca, M. Spasova, M. Farle, M. Hilgendorf, and F. Caruso, J. Magn. Magn. Mater. **240**, 44 (2002).
[12] Y. Saado, M. Golosovsky, D. Davidov, and A. Frenkel, Phys. Rev. B **66**, 195108 (2002).
[13] M. Golosovsky, Y. Saado, and D. Davidov, Appl. Phys. Lett. **75**, 4168 (1999).
[14] M. A. Hayes, N. A. Polson, and A. A Garcia, Langmuir **17**, 2866 (2001).
[15] Ping Sheng, *Scattering and Localization of Classical Waves in Random Media* (World Scientific, Singapore, 1990).
[16] S. Fan, P. R. Villeneuve, and J. D. Joannopoulos, Phys. Rev. B **54**, 11 245 (1996).
[17] M. M. Sigalas, C. T. Chan, K. M. Ho, and C. M. Soukoulis, Phys. Rev. B **52**, 11 744 (1995).
[18] M. M. Sigalas, C. M. Soukoulis, C. T. Chan, R. Biswas, and K. M. Ho, Phys. Rev. B **59**, 12 767 (1999).
[19] V. D. Freilikher, B. A. Liansky, I. V. Yurkevich, A. A. Maradudin, and A. R. McGurn, Phys. Rev. E **51**, 6301 (1995).
[20] L. I. Deych, D. Zaslavsky, and A. A. Lisyansky, Phys. Rev. Lett. **81**, 5390 (1998).
[21] M. Bayindir, E. Cubukcu, I. Bulu, T. Tut, E. Ozbay, and C. M. Soukoulis, Phys. Rev. B **64**, 195113 (2001).
[22] A. A. Asatryan, P. A. Robinson, L. C. Botten, R. C. McPhedran, N. A. Nicorovici, and C. Martijn de Sterke, Phys. Rev. E **60**, 6118 (1999); **62**, 5711 (2000).
[23] V. Yannopapas, N. Stefanou, and A. Modinos, Phys. Rev. Lett. **86**, 4811 (2001).
[24] M. A. Kaliteevski, J. Manzanares Martinez, D. Cassagne, and J. P. Albert, Phys. Rev. B **66**, 113101 (2002); Phys. Status Solidi A **195**, 612 (2003).
[25] Z. Daozhong, H. Wei, Z. Youlong, L. Zhaolin, C. Bingying, and Y. Guozhen, Phys. Rev. B **50**, 9810 (1994).
[26] A. Kondilis and P. Tzanetakis, Phys. Rev. B **46**, 15426 (1992); J. Opt. Soc. Am. A **11**, 1661 (1994).
[27] C. Martijn de Sterke and R. C. McPhedran, Phys. Rev. B **47**, 7780 (1993).
[28] S. A. Bulgakov and M. Nieto-Vesperinas, Waves Random Media **7**, 183 (1997); J. Opt. Soc. Am. A **15**, 503 (1998).
[29] A. Kondilis, Phys. Rev. B **55**, 14 214 (1997).
[30] A. A. Chabanov, M. Stoytchev, and A. Z. Genack, Nature (London) **404**, 850 (2000); M. Stoytchev and A. Z. Genack, Phys. Rev. B **55**, R8617 (1997).
[31] M. E. Zoorob, M. D. B. Charlton, G. J. Parker, J. J. Baumberg, and M. C. Netti, Nature (London) **404**, 740 (2000).
[32] Z. Y. Li and Z. Q. Zhang, Adv. Mater. (Weinheim, Ger.) **13**, 433 (2001).
[33] O. Levy, Phys. Rev. E **61**, 5385 (2000).
[34] M. Golosovsky, Y. Neve-Oz, D. Davidov, and A. Frenkel, Phys. Rev. B **70**, 115105 (2004).
[35] A. Ghazali and J. C. Levy, Phys. Rev. B **67**, 064409 (2003).
[36] R. E. Kusner, J. A. Mann, and A. J. Dahm, Phys. Rev. B **51**, 5746 (1995).
[37] M. Golosovsky, Y. Neve-Oz, and D. Davidov, Synth. Met. **139**, 705 (2003).
[38] A. I. Larkin and Yu. N. Ovchinnikov, J. Low Temp. Phys. **34**, 409 (1979).
[39] L. D. Landau and E. M. Lifshitz, *Statistical Physics* (Pergamon, New York, 1980).
[40] A. M. Portis, *Electromagnetic Fields: Sources and Media* (Wiley, New York, 1978), Chap. 14. p. 562.
[41] S. A. Tretyakov, A. J. Viitanen, S. I. Maslovski, and I. E. Sarela, IEEE Trans. Antennas Propag. **51**, 2073 (2003).
[42] H. C. van de Hulst, *Light Scattering by Small Particles* (Wiley, New York, 1957).
[43] C. F. Bohren and D. R. Huffman, *Absorption and Scattering of Light by Small Particles* (Wiley, New York, 1998).
[44] The local field factor in dipole arrays is closely related to the dipole energy per site. In particular, for highly symmetrical three-dimensional dipole arrays, $A=1$. For the planar dipole array, the local field factor depends on the orientation of the dipoles with respect to the array plane. For the out-of-plane orientation, the lattice sum calculations (Refs. 35 and 36) yield $A=-1.037$ for the hexagonal lattice, and $A=-1.053$ for the square lattice. For the in-plane orientation, $A_{sq}=0.56$ for the square lattice (Ref. 41). We are not familiar with the corresponding calculation for the hexagonal dipole array, but the estimate accounting for the contribution from the close neighbors suggests $A_{hex}\approx 0.5$. Since the local field factor is different for the square and hexagonal lattice, it should be sensitive to shear deformations.
[45] J. B. Pendry, Adv. Phys. **43**, 461 (1994).
[46] P. Yeh, *Optical Waves in Layered Media* (Wiley, New York, 1988).
[47] L. D. Landau and E. M. Lifshitz, *Electrodynamics of Continuous Media* (Pergamon, New York, 1975).
[48] G. D. Cody, T. Tiedje, B. Abeles, B. Brooks, and Y. Goldstein, Phys. Rev. Lett. **47**, 1480 (1981).
[49] S. G. Romanov and C. M. Sotomayor Torres, Phys. Rev. E **69**, 046611 (2004).
[50] V. M. Bedanov, G. V. Gadyak, and Yu. E. Lozovik, Phys. Lett. **92A**, 400 (1982).
[51] K. Zahn, R. Lenke, and G. Maret, Phys. Rev. Lett. **82**, 2721 (1999).
[52] R. Bubeck, C. Bechinger, S. Neser, and P. Leiderer, Phys. Rev. Lett. **82**, 3364 (1999).
[53] J. J. Weiss, J. Phys.: Condens. Matter **15**, S1471 (2003).
[54] M. Kong, B. Partoens, and F. M. Peeters, Phys. Rev. E **67**, 021608 (2003).
[55] G. W. Mulholland, C. F. Bohren, and K. A. Fuller, Langmuir **10**, 2533, (1994).
[56] T. H. Ji, V. G. Lirtsman, Y. Avny, and D. Davidov, Adv. Mater. (Weinheim, Ger.) **13**, 1253 (2001).
[57] J. E. Martin, K. M. Hill, and C. P. Tigges, Phys. Rev. E **59** 5676 (1999).
[58] S. Y. Yang, Y. P. Chiu, B. Y. Jeang, H. E. Horng, C. Y. Hong, and H. C. Yang, Appl. Phys. Lett. **79**, 2372 (2001).
[59] C. Y. Hong, Y. S. Yeh, S. Y. Yang, H. E. Horng, and H. C. Yang, J. Magn. Magn. Mater. **283**, 229 (2004).
[60] In our preliminary study (Ref. 37) we made an attempt to explain our results by Eq. (6), assuming a single crystalline particle array. In fact, our results are better described by Eq. (9) which assumes a polycrystalline particle array.